Experimental Study for ICF-Related Richtmyer-Meshkov Instabilities

B. Motl, J. Niederhaus, D. Ranjan, J. Oakley, M. Anderson, R. Bonazza

November 2006

UWFDM-1320

Presented at the 17th ANS Topical Meeting on Fusion Energy, 13-15 November 2006, Albuquerque NM.

FUSION TECHNOLOGY INSTITUTE

UNIVERSITY OF WISCONSIN

MADISON WISCONSIN

Experimental Study for ICF-Related Richtmyer-Meshkov Instabilities

B. Motl, J. Niederhaus, D. Ranjan, J. Oakley, M. Anderson, R. Bonazza

Fusion Technology Institute
University of Wisconsin
1500 Engineering Drive
Madison, WI 53706

http://fti.neep.wisc.edu

November 2006

UWFDM-1320

Presented at the 17th ANS Topical Meeting on Fusion Energy, 13-15 November 2006, Albuquerque NM.

EXPERIMENTAL STUDY FOR ICF-RELATED RICHTMYER-MESHKOV INSTABILITIES

Bradley Motl, John Niederhaus, Devesh Ranjan, Jason Oakley, Mark Anderson, and Riccardo Bonazza

University of Wisconsin-Madison, Department of Engineering Physics
1500 Engineering Drive, Madison, WI 53706
bonazza@engr.wisc.edu

Richtmyer-Meshkov experiments for a membrane-less, sinusoidal gas interface are carried out in a vertical shock tube for a pre-shock Atwood number ($A=(\rho_2-\rho_1)/(\rho_1+\rho_2)$) of approximately 0.68 at $M = 1.26$ and $M = 2.05$. The perturbation amplitude is obtained by analyzing a time sequence of pre-shock and post-shock images. The Mikaelian and Dimonte and Schneider models both predict the observed growth in the perturbation amplitude, with better agreement obtained for the data at $M = 1.26$.

I. INTRODUCTION

In the inertial confinement (ICF) environment, shock-driven hydrodynamic instabilities and the associated mixing, impose a limit on the efficiency with which fuel material may be compressed to the densities required for fusion, reducing the obtainable fusion yield. These instabilities arise at density nonuniformities and material interfaces as ablative and radiatively-driven shocks pass through the material. In the present work, the phenomenology, mechanisms, and spatial and temporal scales of shock-driven instabilities are investigated using experiments in a gas shock tube environment. In the shock tube environment, hydrodynamic phenomena may be characterized much more precisely than at ICF conditions, due to differences in energy, length, and time scales. Further, the absence of electric and magnetic fields, phase changes, and radiation allows purely hydrodynamic effects to be studied independently. Here, geometric length scales of the deformed interfaces are measured as indications of shock-induced mixing.

Shock-driven hydrodynamic instabilities are present in multi-component flows subjected to acceleration by shock waves. Vorticity (ω) is deposited on a material interface baroclinically during the shock passage due to the misalignment of pressure (p) and density (ρ),

$$\frac{D\omega}{Dt} = \frac{1}{\rho^2}(\nabla\rho \times \nabla p) \qquad (1)$$

causing the interface to become unstable and deform. The geometric features of the deformed interface and mixing zone are studied for a planar interface with a small-amplitude sinusoidal perturbation. This class of problems is called the Richtmyer-Meshkov[1,2] (RM) instability, and the evolution is depicted in Fig. 1. The growth sequence was summarized by Brouillette[3], with the deposited vorticity (indicated in Fig. 1b) causing the initial amplitude of the perturbation to grow linearly. The linear amplitude growth is followed by a nonlinear growth regime (Fig. 1c). The nonlinear growth is followed by a regime that is influenced by the Kelvin-Helmholtz instability, which causes roll-up structures on each side of the heavy fluid spike and results in the formation of mushroom-shaped structures (Fig. 1d). The complex nature of these vortices ultimately leads to the development of a turbulent mixing zone (Fig. 1e).

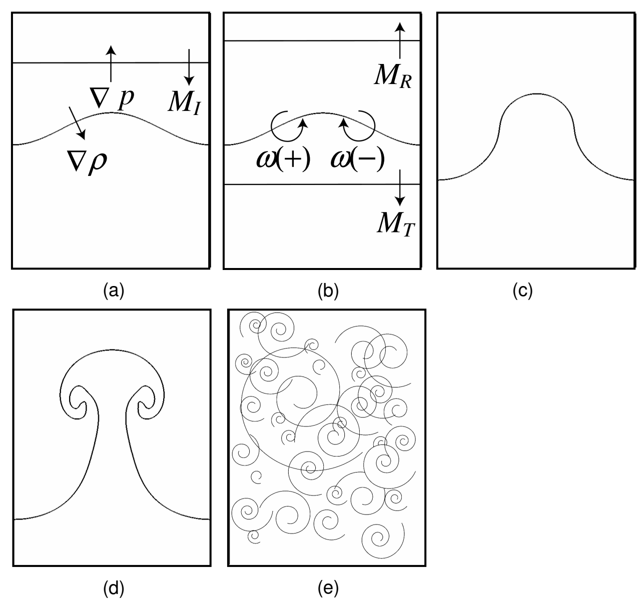

Fig. 1. The evolution of the Richtmyer-Meshkov instability: (a) initial configuration just prior to shock arrival for an $A > 0$ scenario, (b) linear growth regime, (c) start of nonlinear growth, (d) appearance of mushroom structures, and (e) turbulent mixing.

In Fig. 1, M_I is the initial shock wave, M_R is the reflected shock wave, and M_T is the transmitted shock wave.

II. EXPERIMENTAL SETUP

The present experimental campaign is carried out at the Wisconsin Shock Tube Laboratory. The shock tube is oriented vertically and is downward firing, and it has a total length of 9.13 m. The driver section is circular in cross section with a radius of 0.41 m, while the driven section has an inner square cross section with 0.25-m sides[4]. A high-pressure boost tank is connected to the driver section by a pneumatically-driven fast-opening valve to control the diaphragm rupture time. Piezoelectric pressure transducers mounted along the shock tube side walls are used to trigger the controlling electronics and to measure the shock speed. The interface preparation method designed and used for this experiment is similar to the one used by Jones and Jacobs[5]. The interface section of the shock tube, shown in Fig. 2, is designed to accommodate two rectangular 5.08×25 cm aluminum pistons which have slots that are connected to a vacuum pump that is set to an outflow rate of 6.67×10^{-4} m^3/s. Sulfur hexafluoride is introduced into the bottom of the shock tube at a flow rate of 1.55×10^{-4} m^3/s, and nitrogen seeded with acetone or smoke is introduced into the shock tube just below the diaphragm at a rate of 5.13×10^{-4} m^3/s. The differences in flow rates account for different shock tube volumes above and below the interface.

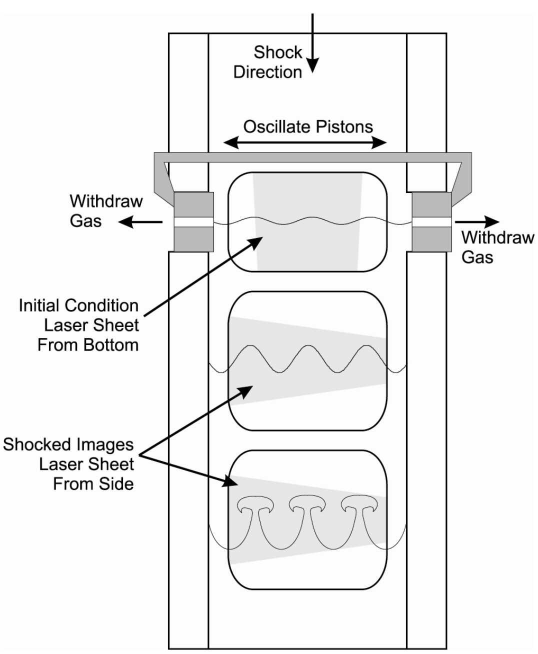

Fig. 2. Schematic of shock tube interface section with the piston system, and imaging windows.

Acetone seeding is performed by running nitrogen through two consecutive acetone baths that are kept at a constant temperature. On average, the mole fraction of acetone in the nitrogen/acetone mixture is 0.11. The pre-shock Atwood number for this interface is 0.64. Smoke seeding is performed by introducing smoke from a port approximately 2 m above the interface. The pre-shock Atwood number for the smoke-seeded N_2 over SF_6 is 0.68.

The gases are continuously flowed for 45 minutes at which point a flat interface with a 1-cm-thick diffusion layer is achieved. To generate a 2-D perturbation on the interface, the pistons are then driven by a stepper motor at a frequency that creates a standing wave. In a nitrogen-acetone mixture, the pistons are oscillated at a frequency of 1.9 Hz for three revolutions ($\lambda \approx 90$ mm wave) or 2.6 Hz for four revolutions ($\lambda \approx 180$ mm wave). For the smoke seeded case, the pistons are oscillated at 2.1 Hz for three revolutions ($\lambda \approx 170$ mm wave). The total piston travel is 2.86 cm. During the piston motion, electronic triggers are sent to open the camera shutters, close the vacuum pump valve, and open the boost tank. A pressure transducer 0.71 m above the interface is used to detect the pressure jump from the shock wave, which then serves as a trigger to fire the lasers at predetermined delay times. For the case of acetone seeding, planar laser-induced fluorescence (PLIF) is used to produce one pre-shock initial condition image and two post-shock images. For the case of smoke seeding, Mie scattering is utilized to generate one pre-shock and one post-shock image.

All pre-shock and post-shock images are corrected for laser beam divergence and attenuation. A region of interest is extracted from a raw image, including either the entire width of the shock tube, or a single wavelength of the perturbation. The image is first corrected for divergence with a conformal mapping algorithm that conservatively maps diverging light rays to parallel columns, and then corrects for laser attenuation (due to absorption) by integrating Beer's Law along these columns. The image is then remapped to physical space, and convolved with a five-pixel Gaussian distribution, to reduce the levels of fine-scale noise in the image due to artifacts of the imaging technique.

This study utilizes the non-dimensional parameters used by Jacobs and Krivets[6]. The non-dimensional amplitude is given as:

$$a = k(\eta - \eta_0^1) \qquad (2)$$

where k is the wavenumber ($2\pi / \lambda$), η is the perturbation amplitude (measured as half the peak to peak amplitude), and η_0^1 is the post-shock initial amplitude. The non-dimensional time is given as:

$$\tau = k\dot{\eta}_0 t \qquad (3)$$

where $\dot{\eta}_0$ is the initial growth rate, and is approximated[6] by:

$$\dot{\eta}_0 \approx k\eta_0^1 A^1 V_0 \qquad (4)$$

where A^1 is the post-shock Atwood number and V_0 is the velocity jump of the interface due to the impulsive acceleration of the shock.

The modal content of the initial condition used in the M = 2.05 experiments is characterized using the following procedure. The initial condition images are corrected as discussed above, and the light intensity, I, is then normalized to [0, 1] in each column and the interface location is designated as the I = 0.5 location. A Fourier transform of the columnar interface locations produces a modal spectrum for the initial condition. The amplitude of each mode is normalized with respect to the maximum amplitude of the perturbation, and six initial interface spectra are averaged to produce the mean modal spectrum shown in Fig. 3.

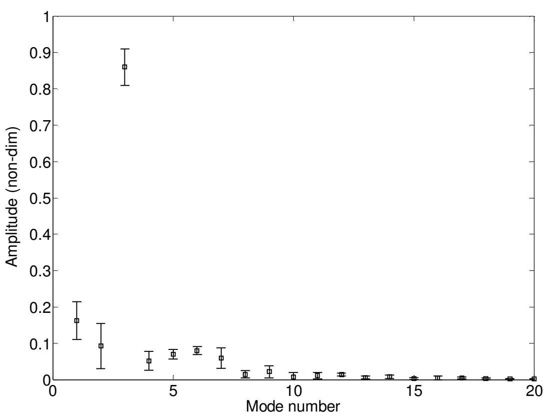

Fig. 3. The mean modal content of the M = 2.05 initial condition interface.

Figure 3 shows that the initial condition used for the experiments is predominantly single-moded. However, it is acknowledged that other modes exist with finite amplitude, the largest of which is approximately 1/5 of the dominant mode.

A three-dimensional reconstruction is performed on the λ=18.0 cm initial condition used for the M = 1.26 experiments. A glass plate is installed on the bottom of the shock tube to allow the planar laser sheet to be placed at five locations within the shock tube. The five locations chosen are: x = 12.70 cm (center), x = 10.36 cm, x = 8.01 cm, x = 5.69 cm, and x = 2.54 cm. For this analysis, it is assumed that the perturbation is symmetric about the center plane (x = 12.70 cm) of the shock tube. Five images are taken at each laser sheet location and then averaged. The averaged initial conditions are then compiled and interpolated to produce the 3-D reconstruction shown in Fig. 4. A planar sheet is indicated at the center of the shock tube where imaging would occur during an experiment. As seen in Fig. 4, the initial condition is two-dimensional in the region of interest (the central portion of the shock tube). Near the walls, however, the perturbation becomes three-dimensional due to viscous effects.

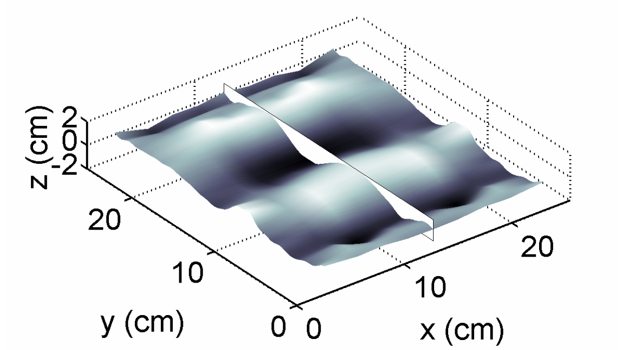

Fig. 4. A 3-D reconstruction of the λ =18.0 cm interface used for the M=1.26 experiments.

III. RESULTS

One pre-shock and two post-shock images are obtained per experiment for the M = 1.26 case where the N_2 is seeded with acetone. Figure 5 is a non-dimensional time sequence of experimental images from a single experiment. The images only represent a small region of imaging plane (10 cm in width).

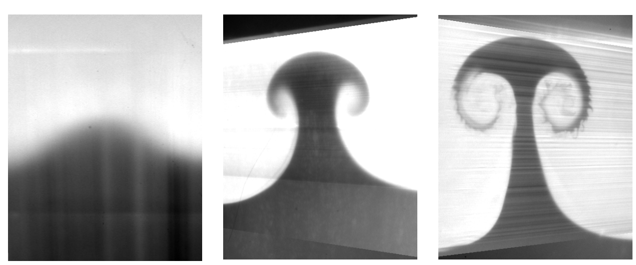

(a) (b) (c)

Fig. 5. Non-dimensional time sequence of M = 1.26 images: (a) τ= 0.00, (b) τ= 4.66, and (c) τ= 8.79.

Figure 5 shows that by τ = 4.66, the growth of the instability has proceeded far into the nonlinear growth regime and by τ = 8.79, fully developed mushroom structures are present. The development of small-scale secondary instabilities on the characteristic rollup structures is apparent in Fig. 5(c) which suggests that a transition to a turbulent mixing zone is occurring.

One pre-shock and one post-shock image is obtained per experiment for the M = 2.05 case where the N_2 is seeded with smoke. Figure 6 is a non-dimensional time sequence of experimental images from multiple experiments. The field of view spans 22.5 cm.

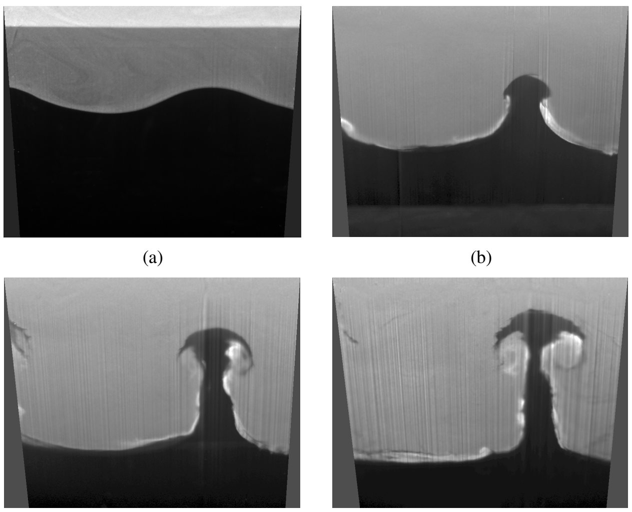

Fig. 6. Non-dimension time sequence of M = 2.05 images: (a) τ = 0.00, (b) τ = 1.54, (c) τ = 3.29, and (d) τ = 3.98.

Figure 6 indicates that for increased shock strength, similar geometric features appear at earlier non-dimensional times. In particular, rollup features appear as early as τ = 3.98 in the M = 2.05 experiments, but are not distinctly seen until much later in the M = 1.26 case. Another difference between the two sets of experimental results is the shape of the downward-growing N_2 bubbles at late times. Figure 5(c) shows a round bubble shape, whereas Fig. 6(c,d) show a distinct flattening of the bubble near the base of the "mushroom" structure.

The experimental data are compared to three analytical models for perturbation amplitude growth due to the RM instability. The empirical model of Sadot *et al.*[7] utilizes experimental parameters and requires knowledge of the initial perturbation spectrum. In the present study, the model of Sadot *et al.* is implemented for the case of an initially single-mode perturbation. The Mikaelian[8] model is an explicit, analytic expression for the evolution of a two-dimensional, single mode interface. Lastly, the Dimonte and Schneider[9] model is a power law model that is designed for a single-mode or multi-mode initial condition.

The experimental amplitude is non-dimensionalized using Eq. 2 and plotted versus the non-dimensional time given in Eq. 3. Figure 7 compares the experimental data to the analytical models described above for the M = 1.26 case, and Fig. 8 is for the M = 2.05 data. The Sadot *et al.* model consistently over-predicts the observed growth for both cases, whereas both the Mikaelian and Dimonte and Schneider models more accurately represent the M = 1.26 experimental data as shown in Fig. 7. However, at late non-dimensional times, both of these models seem to under-predict the experimental data, though it is difficult to make any firm conclusion due to the lack of data points at τ > 6.0. For the case of M = 2.05, the experimental data shown in Fig. 8 fall between the Mikaelian model (which tends to over-predict the growth) and the Dimonte and Schneider model (which tends to under-predict the growth).

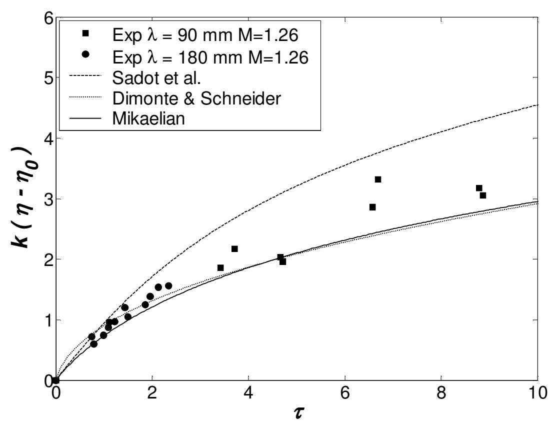

Fig. 7. Non-dimensional amplitude versus time for the M = 1.26 experiments compared to three models.

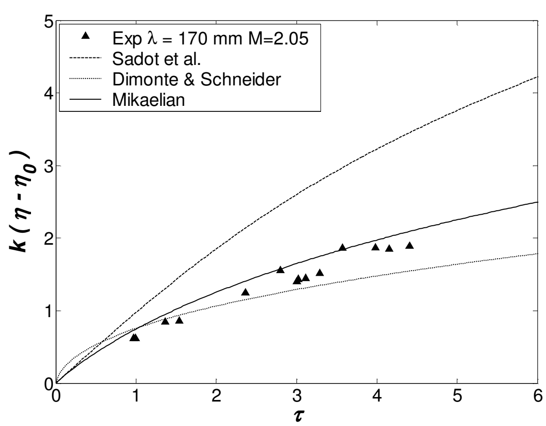

Fig. 8. Non-dimensional amplitude versus time for the M = 2.05 experiments compared to three models.

IV. CONCLUSIONS

The experimental method presented in this paper is adequate for creating a predominantly single-mode interface that is two-dimensional within a region of interest. The images and data obtained from these experiments provide a useful set of experimental data for the modeling of shock-induced mixing. Thus far, the results have indicated the accuracy of several nonlinear models for Richtmyer-Meshkov growth, including in particular the Mikaelian model. Future work will yield additional insights as to the mechanisms for the observed differences.

ACKNOWLEDGMENTS

The authors would like to express sincere thanks to Paul Brooks (UW-Madison) for developing and maintaining the experimental setup. This work was supported by US DOE Grant # DE-FG52-03NA00061.

REFERENCES

1. R. D. RICHTMYER, *Comm. on Pure and Appl. Math*. **13**, 297 (1960).
2. Y. Y. MESHKOV, NASA Technical Translation **NASA TT F-13,074** (1970).
3. M. BROUILLETTE, *Ann. Rev. Fluid Mech.,* **34,** 445 (2002).
4. M. H. ANDERSON, B. P. PURANIK, J. G. OAKLEY, P. W. BROOKS and R. BONAZZA, *Shock Waves*, **10**, 377 (2000).
5. M. A. JONES and J. W. JACOBS, *Phys. Fluids* **9 (10)**, 3078 (1997).
6. J. W. JACOBS and V. V. KRIVETS, *Phys. Fluids* **17 (3)**, 034105-1 (2005).
7. O. SADOT *et al.*, *Phys. Rev. Lett.*, **80 (8)**, 1654 (1998).
8. K. O. MIKAELIAN, *Phys. Rev. E*, **67 (2)**, 026319-1 (2003).
9. G. DIMONTE and M. SCHNEIDER, *Phys. Fluids*, **12 (2)**, 304 (2000).